Environ Sci Pollut Res (2018) 25:2691–2701
https://doi.org/10.1007/s11356-017-0701-z

RESEARCH ARTICLE

The removal of COD and NH_3-N from atrazine production wastewater treatment using UV/O_3: experimental investigation and kinetic modeling

Liang Jing[1] · **Bing Chen**[1,2] · **Diya Wen**[2] · **Jisi Zheng**[1] · **Baiyu Zhang**[1]

Received: 30 June 2017 / Accepted: 6 November 2017 / Published online: 13 November 2017

Abstract In this study, a UV/O_3 hybrid advanced oxidation system was used to remove chemical oxygen demand (COD), ammonia nitrogen (NH_3-N), and atrazine (ATZ) from ATZ production wastewater. The removal of COD and NH_3-N, under different UV and O_3 conditions, was found to follow pseudo-first-order kinetics with rate constants ranging from 0.0001–0.0048 and 0.0015–0.0056 min^{-1}, respectively. The removal efficiency of ATZ was over 95% after 180 min treatment, regardless the level of UV power. A kinetic model was further proposed to simulate the removal processes and to quantify the individual roles and contributions of photolysis, direct O_3 oxidation, and hydroxyl radical (OH·) induced oxidation. The experimental and kinetic modeling results agreed reasonably well with deviations of 12.2 and 13.1% for the removal of COD and NH_3-N, respectively. Photolysis contributed appreciably to the degradation of ATZ, while OH· played a dominant role for the removal of both COD and NH_3-N, especially in alkaline environments. This study provides insights into the treatment of ATZ containing wastewater using UV/O_3 and broadens the knowledge of kinetics of ozone-based advanced oxidation processes.

Keywords Atrazine production wastewater · UV/O_3 · Chemical oxygen demand · Ammonia nitrogen · Hydroxyl radical · Kinetic modeling

Responsible editor: Vítor Pais Vilar

Electronic supplementary material The online version of this article (https://doi.org/10.1007/s11356-017-0701-z) contains supplementary material, which is available to authorized users.

✉ Bing Chen
bchen@mun.ca

[1] Northern Region Persistent Organic Pollution Control (NRPOP) Laboratory, Faculty of Engineering and Applied Science, Memorial University of Newfoundland, St. John's, NL A1B 3X5, Canada

[2] Key Laboratory of Regional Energy and Environmental Systems Optimization, Ministry of Education, Resources and Environmental Research Academy, North China Electric Power University, Beijing 102206, China

Introduction

Atrazine (ATZ) is a chloro-s-triazine herbicide that has been widely used for the control of broad leaf and grassy weeds by interfering with the normal function of photosynthesis. Due to its high leaching potential, resistance to microbial degradation, slow hydrolysis, and moderate solubility, ATZ can accumulate in soil, surface water, and groundwater for a long period of time after being applied. ATZ can cause genotoxicity, thyroid gland problems, endocrine disruption, and serious human birth defects such as low birth weights and menstrual problems (Kong et al. 2016). U.S. EPA has classified ATZ as a possible human carcinogen, priority hazardous substance, and endocrine-disrupting compound. Aside from leaching after application, another important source of ATZ comes from the inadequate disposal of wastewater during its production process as its removal through traditional wastewater treatment processes is often incomplete (da Costa Filho et al. 2016; Aquino et al. 2017). Therefore, reliable and effective techniques for removing ATZ from industrial wastewater, especially from its production wastewater, are much desirable as a source control measure.

Recently, many research efforts have been focused on the removal of ATZ from aqueous environments using either stand-alone or hybrid advanced oxidation processes (AOPs), such as UV irradiation (Silva et al. 2014; Aquino et al. 2017), ozonation (Acero et al. 2000; Beltrán et al.

2000; Yang et al. 2014; Zhou et al. 2016; Gomes et al. 2017), UV/ozonation (Beltrán et al. 1994), sonolysis (Xu et al. 2014), Fenton process (Zhao et al. 2014), UV/H_2O_2 (Beltrán et al. 1996; Luo et al. 2015a), UV/chlorine (Kong et al. 2016), and UV/persulfate (Khan et al. 2014; Bu et al. 2016). The degradation of ATZ by AOPs usually involves de-chlorination, de-alkylation, and de-amination with subsequent hydroxylation, leading to the main products including cyanuric acid, ammelide, and ammeline (Bianchi et al. 2006). AOPs cannot achieve complete mineralization because opening the s-triazine ring (e.g., cyanuric acid) is difficult and can only be achieved under hydrothermal conditions (Horikoshi and Hidaka 2003). Nonetheless, effluent from AOPs can be readily treated by following biological treatment in order to completely mineralize ATZ and its end products (Lester et al. 2013). It should be noted that most of the previous studies reported in the literature have been performed in the background of ultrapure water, drinking and natural water, or synthetic wastewater. The effectiveness of AOPs in treating ATZ containing industrial wastewater particularly ATZ production wastewater has not been documented.

Given the industrial synthesis of ATZ needs a high amount of sodium hydroxide to avoid acidification, the ATZ production wastewater can be considered as a concentrated solution of sodium hydroxide contaminated with ATZ and other organics. The recovery of high-purity sodium hydroxide is thus an attractive option from a waste management perspective and therefore requires the reduction of impurities such as chemical oxygen demand (COD) in industry practice (Prieto-Rodríguez et al. 2013; Manenti et al. 2015). Ammonia nitrogen (NH_3-N) present in ATZ production wastewater also needs to be reduced in order to protect aquatic organisms at receiving water bodies (Huang et al. 2008; Khuntia et al. 2012; Wen et al. 2016). To the best of our knowledge, there exists no previous report of the simultaneous removal of COD, NH_3-N, and ATZ from ATZ containing industrial wastewater by AOPs. In addition, kinetic modeling has been proposed as an efficient tool to enhance the understanding of the mechanisms of AOPs and to aid the design and optimization of industrial applications (Yang et al. 2014; Bu et al. 2016; Zhou et al. 2016). However, there have been no such studies thus far in modeling the treatment of ATZ containing wastewater by AOPs.

To help fill the knowledge gaps, the objectives of the present work were (1) to investigate the efficacy of ATZ production wastewater treatment, particularly the removal of COD and NH_3-N by a typical AOP, namely UV/O_3; (2) to develop a mathematical model for the removal kinetics of COD, NH_3-N, and ATZ; and (3) to compare the contributions of direct O_3 oxidation and indirect radical oxidation in the treatment system.

Materials and methods

Chemicals and photoreactor

Potassium dichromate, sulfuric acid, silver sulfate, mercuric sulfate, ferroin, ammonium iron sulfate, sodium hydroxide, salicylic acid, potassium sodium tartrate, sodium pentacyanonitrosylferrate, and sodium hypochlorite were purchased from Beijing Chemical Works, China. Atrazine-d5 standard and sodium thiosulfate were purchased from Anpel Laboratory Technologies (Shanghai), China. Trichlo romethane (Thermo Fisher Scientific, China) was used for aqueous sample extraction. All chemicals were of analytical reagent grade (> 99% pure) and used as received without further purification. Ultrapure water was produced on-site from a Direct-Q 3 UV unit (Millipore, France). ATZ production wastewater was collected from a pesticide manufacturer. Detailed location information is not available due to client confidentiality. Its physical-chemical characteristics are listed in Table 1.

As shown in Fig. S1 (Supplementary Material), the bench-scale photoreactor has an inner 4 L quartz jar and an outer stainless steel jacket. The outer jacket has an aluminum lid that can be sealed to provide heat and light insulation. The inner diameter, height, and wall thickness of the quartz jar are 20, 25, and 0.4 cm, respectively. Eight 3.5 W low-pressure UV lamps, emitting exclusively at 254 nm, are evenly mounted inside the quartz jar near the wall. Incident irradiance for different numbers of lamps was measured at a wavelength of 254 nm with a calibrated radiometer (Sentry Optronics Corp, Model ST-512). A 300-W ozone generator with dedicated ozone flow rate monitor is used to produce ozone on-site from ambient air. The inner quartz jar has a PTFE lid equipped with a stirring rod on which two PTFE six-bladed paddle impellers are mounted to stir the wastewater sample at 80 rpm.

Table 1 Detailed physical-chemical characteristics of the ATZ production wastewater

Parameter	Value	Unit
pH	12	–
ATZ	5	mg L^{-1}
NH_3-N	24.5	mg L^{-1}
COD	14,300	mg L^{-1}
Chlorides	197,500	mg L^{-1}
TSS	1890	mg L^{-1}
BOD_5	3850	mg L^{-1}
Phosphate	0.57	mg L^{-1}
Aniline	0.55	mg L^{-1}
Toluene	11.2	mg L^{-1}
Chromaticity	< 1	–

Table 2 Reactions occurred in the UV/O_3 system

UV/O_3 reactions	Reaction constants	Reference
$O_3 + H_2O + h\nu \rightarrow H_2O_2 + O_2$	$\Phi_{O_3} = 0.64$ mol E^{-1}	Beltrán et al. (2000)
$ATZ + h\nu \rightarrow$ products	$\Phi_{Atz} = 0.04$ mol E^{-1}	Khan et al. (2014)
$H_2O_2 + h\nu \rightarrow 2OH\cdot$	$\Phi_{H_2O_2} = 0.5$ mol E^{-1}	Beltrán et al. (2000)
$H_2O_2 \leftrightarrow HO_2^- + H^+$	$pK_a = 11.8$	Andreozzi et al. (1999)
$HO_2^- + h\nu \rightarrow OH\cdot + O^-$	$\Phi_{HO_2^-} = 0.5$ mol E^{-1}	Andreozzi et al. (1999)
$O_3 + ATZ \rightarrow$ products	$k_1 = 6\ M^{-1}\ s^{-1}$	Acero et al. (2000)
$O_3 + HO_2^- \rightarrow OH\cdot + O_2 + O_2^-\cdot$	$k_2 = 2.8 \times 10^6\ M^{-1}\ s^{-1}$	Staehelin and Hoigne (1982)
$O_3 + OH^- \rightarrow HO_2^- + O_2$	$k_3 = 70\ M^{-1}\ s^{-1}$	Staehelin and Hoigne (1982)
$O_3 + H_2O_2 \rightarrow OH\cdot + HO_2\cdot + O_2$	$k_4 = 1 \times 10^{-2}\ M^{-1}\ s^{-1}$	Neta et al. (1988)
$O_3 + OH\cdot \rightarrow HO_2\cdot + O_2$	$k_5 = 1.1 \times 10^8\ M^{-1}\ s^{-1}$	Neta et al. (1988)
$H_2O_2 + OH\cdot \rightarrow HO_2\cdot + H_2O$	$k_6 = 2.7 \times 10^7\ M^{-1}\ s^{-1}$	Beltrán et al. (1996)
$HO_2^- + OH\cdot \rightarrow HO_2\cdot + OH^-$	$k_7 = 7.5 \times 10^9\ M^{-1}\ s^{-1}$	Buxton et al. (1988)
$HO_2\cdot + OH\cdot \rightarrow H_2O + O_2$	$k_8 = 6.6 \times 10^9\ M^{-1}\ s^{-1}$	Garoma and Gurol (2004)
$ATZ + OH\cdot \rightarrow$ products	$k_9 = 3 \times 10^9\ M^{-1}\ s^{-1}$	Lutze et al. (2015)
$Cl^- + OH\cdot \leftrightarrow ClOH^-\cdot$	$k_{10f} = 4.3 \times 10^9\ M^{-1}\ s^{-1}$	Kong et al. (2016)
	$k_{10r} = 6 \times 10^9\ s^{-1}$	Kong et al. (2016)
$ClOH^-\cdot \rightarrow Cl\cdot + OH^-$	$k_{11} = 23\ s^{-1}$	Luo et al. (2015a)
$ClOH^-\cdot + Cl^- \rightarrow Cl_2^-\cdot + OH^-$	$k_{12} = 1 \times 10^5\ M^{-1}\ s^{-1}$	Luo et al. (2015a)
$Cl\cdot + Cl^- \rightarrow Cl_2^-\cdot$	$k_{13f} = 8.5 \times 10^9\ M^{-1}\ s^{-1}$	Fang et al. (2014)
	$k_{13r} = 1.1 \times 10^5\ s^{-1}$	Fang et al. (2014)
$Cl\cdot + H_2O_2 \rightarrow HO_2\cdot + Cl^- + H^+$	$k_{14} = 2 \times 10^9\ M^{-1}\ s^{-1}$	Yu and Barker (2003)
$Cl_2^-\cdot + H_2O_2 \rightarrow HO_2\cdot + 2Cl^- + H^+$	$k_{15} = 1.4 \times 10^5\ M^{-1}\ s^{-1}$	Matthew and Anastasio (2006)
$Cl_2^-\cdot + ATZ \rightarrow products$	$k_{16} = 5 \times 10^4\ M^{-1}\ s^{-1}$	Luo et al. (2015a)
$Cl^- + O_3 \rightarrow ClO^- + O_2$	$k_{17} = 3 \times 10^{-3}\ M^{-1}\ s^{-1}$	Kang et al. (2008)
$Cl_2^-\cdot + O_3 \rightarrow ClO\cdot + Cl^- + O_2$	$k_{18} = 9 \times 10^7\ M^{-1}\ s^{-1}$	Bielski (1993)
$COD + OH\cdot \rightarrow$ products	$k_{19} = 4.9 \times 10^8\ M^{-1}\ s^{-1}$	Mohajerani et al. (2012)
$COD + O_3 \rightarrow$ products	$k_{20} = 0.32\ M^{-1}\ s^{-1}$	Rivas et al. (2009)
	$k_{21} = 0.5\ M^{-1}\ s^{-1}$	Haag et al. (1984)
$NH_3 + OH\cdot \rightarrow NH_2\cdot + H_2O$	$k_{22} = 3 \times 10^8\ M^{-1}\ s^{-1}$	Huang et al. (2008)
$NH_2\cdot + H_2O_2 \rightarrow NHOH\cdot + H_2O$	$k_{23} = 9.1 \times 10^7\ M^{-1}\ s^{-1}$	Huang et al. (2008)
$NHOH\cdot + HO_2^- \rightarrow NH_2O_2^- + OH\cdot$	$k_{24} = 3.6 \times 10^8\ M^{-1}\ s^{-1}$	Huang et al. (2008)
$NH_3 + 4O_3 \rightarrow NO_3^- + H^+ + H_2O + 4O_2$		
NH_3 stripping	$k_{25} = 3.47 \times 10^{-6}\ s^{-1}$	Park and Kim (2015)

Experimental procedure and analytical methods

The experimental procedure started by transferring 2 L ATZ production wastewater into the quartz jar and stirring it for 20 min to reach the thermal and volatilization equilibria. Then, the ozone generator was switched on and O_3 was bubbled into the bottom of the quartz jar through a distributor nozzle at a fixed rate of 15 g h^{-1} (measured by the ozone generator). UV lamps were switched on 30 min before filling the jar, and power was provided at three different levels of 0, 7, and 14 W by using 0, 2, and 4 lamps, respectively. Temperature was maintained at room temperature and the system was magnetically stirred during the experiment. At various time intervals during a 180-min period, a 20-mL water sample was collected from the reactor using a peristaltic pump, transferred into a 20-mL amber vial and immediately quenched by adding 1.0 mL saturated $Na_2S_2O_3$ solution to remove residual oxidants. All experiments were triplicated and averaged to ensure reproducibility.

Given the removal efficiency of ATZ by UV/O_3 was investigated in our previous studies (Jing et al. 2015, 2017), the focus of this study was on the reduction kinetics of COD and NH_3-N. Therefore, the measurement of COD and NH_3-N was conducted for samples collected at all time points (i.e., 20, 40, 60, 90, 120, 150, and 180 min). COD was measured by the potassium dichromate method after 100-fold dilution due to the high chloride content. NH_3-N was determined by the spectrophotometer method with salicylic acid. Contrastingly, ATZ was only measured at the ending point (i.e., 180 min) by a pretreatment method proposed by Zheng et al. (2015a) and a

gas chromatograph (GC) (Agilent 7890A) equipped with a HP-5MS column (30 m × 5 mm × 0.25 μm) and a mass selective detector (MS) (Agilent 5975C). Oven temperature was initially set as 70 °C for 2 min and then increased by 20 °C min^{-1} to 230 °C and maintained for 20 min. Analysis was performed in the selected ion monitoring mode at an electron energy of 70 eV and a source temperature of 230 °C.

Kinetic modeling

Table 2 summarizes the possible reactions in the UV/O_3 batch reaction system along with rate constants obtained from the literature. To develop the kinetic model, the following assumptions were made: (1) only reactions tabulated in Table 2 occurred in the system; (2) to account for light scattering and absorbing effect caused by suspended solids, a linear attenuation correlation suggested by Luo and Al-Dahhan (2004) and Benson and Rusch (2006) was adopted to modify the Beer-Lambert Law equation as shown in Eq. 5; (3) the reactions of COD with O_3 and OH· were second order; (4) the removal of COD caused by direct photolysis was negligible as compared with oxidation by OH· and O_3 (Gassie et al. 2016); (5) NH_3-N was expressed in the form of NH_3 because at pH greater than 11, over 90% NH_3-N exists as free ammonia (Khuntia et al. 2012); (6) the radical scavenging effect caused by CO_3^{2-} and HCO_3^- was negligible due to the complex matrix (Luo et al. 2015a); (7) the change of pH was negligible; (8) given the flow rate of 15 g h^{-1} and the total volume of 2 L in this study, an ozone injection rate of 4.34×10^{-5} M s^{-1} was obtained. Ozone mass transfer rate in semi-batch reactors usually stabilizes after a certain period of time. However, in this study, the real-time ozone concentration was not measured due to turbidity and technical difficulties. To address this concern, as shown in Eq. 7, a fixed ozone utilization rate of 0.7 (Pophali et al. 2011; Quero-Pastor et al. 2014) was adopted to represent the increase of ozone concentration; (9) according to Park and Kim (2015), a pseudo-first-order rate constant of 3.47×10^{-6} s^{-1} was used for ammonia stripping; (10) because the wastewater pH (i.e., 12) was greater than the pK_a (i.e., 11.8) of H_2O_2, the existence of its conjugated species (HO_2^-) and the high extinction coefficient of HO_2^- (i.e., 240 M^{-1} cm^{-1}) cannot be overlooked.

The kinetic expressions of ATZ, O_3, OH·, H_2O_2, HO_2, HO_2^-, Cl^-, Cl, Cl_2^-, $ClOH^-$, COD, NH_3, NH_2, and NHOH· are shown in Eqs. 1–13 as below and Eqs. S1–S6 in the Supplementary Material, with the reaction rate constants listed in Table 2.

$$f_{ATZ} = \frac{\varepsilon_{ATZ}[ATZ]}{\varepsilon_{ATZ}[ATZ] + \varepsilon_{O_3}[O_3] + \varepsilon_{H_2O_2}[H_2O_2] + \varepsilon_{HO_2^-}[HO_2^-]} \quad (1)$$

$$f_{O_3} = \frac{\varepsilon_{O_3}[O_3]}{\varepsilon_{ATZ}[ATZ] + \varepsilon_{O_3}[O_3] + \varepsilon_{H_2O_2}[H_2O_2] + \varepsilon_{HO_2^-}[HO_2^-]} \quad (2)$$

$$f_{H_2O_2} = \frac{\varepsilon_{H_2O_2}[H_2O_2]}{\varepsilon_{ATZ}[ATZ] + \varepsilon_{O_3}[O_3] + \varepsilon_{H_2O_2}[H_2O_2] + \varepsilon_{HO_2^-}[HO_2^-]} \quad (3)$$

$$f_{HO_2^-} = \frac{\varepsilon_{HO_2^-}[HO_2^-]}{\varepsilon_{ATZ}[ATZ] + \varepsilon_{O_3}[O_3] + \varepsilon_{H_2O_2}[H_2O_2] + \varepsilon_{HO_2^-}[HO_2^-]} \quad (4)$$

$$I = I_0 e^{-\alpha b} = I_0 e^{-(k_b c_b + k_w) b} \quad (5)$$

$$d[ATZ]/dt = -\Phi_{ATZ} I f_{ATZ}\left(1 - e^{-2.303b\left(\varepsilon_{ATZ}[ATZ] + \varepsilon_{O_3}[O_3] + \varepsilon_{H_2O_2}[H_2O_2] + \varepsilon_{HO_2^-}[HO_2^-]\right)}\right) - k_1[O_3][ATZ] - k_9[ATZ][OH\cdot] - k_{16}[ATZ][Cl_2^-\cdot] \quad (6)$$

$$d[O_3]/dt = 0.7 \times 4.34 \times 10^{-5} - \Phi_{O_3} I f_{O_3}\left(1 - e^{-2.303b\left(\varepsilon_{ATZ}[ATZ] + \varepsilon_{O_3}[O_3] + \varepsilon_{H_2O_2}[H_2O_2] + \varepsilon_{HO_2^-}[HO_2^-]\right)}\right) - k_1[O_3][ATZ] - k_2[O_3][HO_2^-] - k_3[O_3][OH^-] - k_4[O_3][H_2O_2] - k_5[O_3][OH\cdot] - k_{17}[O_3][Cl^-] - k_{18}[O_3][Cl_2^-\cdot] - k_{20}[O_3][COD] - 4 \times k_{21}[O_3][NH_3] \quad (7)$$

$$d[OH\cdot]/dt = 2\Phi_{H_2O_2} I f_{H_2O_2}\left(1 - e^{-2.303b\left(\varepsilon_{ATZ}[ATZ] + \varepsilon_{O_3}[O_3] + \varepsilon_{H_2O_2}[H_2O_2] + \varepsilon_{HO_2^-}[HO_2^-]\right)}\right) + \Phi_{HO_2^-} I f_{HO_2^-}\left(1 - e^{-2.303b\left(\varepsilon_{ATZ}[ATZ] + \varepsilon_{O_3}[O_3] + \varepsilon_{H_2O_2}[H_2O_2] + \varepsilon_{HO_2^-}[HO_2^-]\right)}\right) + k_2[O_3][HO_2^-] - k_4[O_3][H_2O_2] - k_5[O_3][OH\cdot] - k_6[H_2O_2][OH\cdot] - k_7[HO_2^-][OH\cdot] - k_8[HO_2\cdot][OH\cdot] + k_9[ATZ][OH\cdot] + k_{10r}[ClOH^-\cdot] - k_{10f}[Cl^-][OH\cdot] - k_{19}[COD][OH\cdot] - k_{22}[NH_3][OH\cdot] + k_{24}[NHOH\cdot][HO_2^-] \quad (8)$$

$$d[H_2O_2]/dt = \Phi_{O_3} I f_{O_3}\left(1-e^{-2.303b\left(\varepsilon_{ATZ}[ATZ]+\varepsilon_{O_3}[O_3]+\varepsilon_{H_2O_2}[H_2O_2]+\varepsilon_{HO_2^-}[HO_2^-]\right)}\right)-\Phi_{H_2O_2} I f_{H_2O_2}$$
$$\left(1-e^{-2.303b\left(\varepsilon_{ATZ}[ATZ]+\varepsilon_{O_3}[O_3]+\varepsilon_{H_2O_2}[H_2O_2]+\varepsilon_{HO_2^-}[HO_2^-]\right)}\right) - k_4[O_3][H_2O_2]-k_6[H_2O_2][OH\cdot]- \quad (9)$$
$$k_{14}[H_2O_2][Cl\cdot]-k_{15}[H_2O_2]\left[Cl_2^-\cdot\right]-k_{23}[NH_2\cdot][H_2O_2]$$

$$d[HO_2\cdot]/dt = k_4[O_3][H_2O_2] + k_5[O_3][OH\cdot] + k_6[H_2O_2][OH\cdot] + k_7\left[HO_2^-\right][OH\cdot]- \quad (10)$$
$$k_8[HO_2\cdot][OH\cdot] + k_{14}[H_2O_2][Cl\cdot] + k_{15}[H_2O_2]\left[Cl_2^-\cdot\right]$$

$$d\left[HO_2^-\right]/dt = -\Phi_{HO_2^-} I f_{HO_2^-}\left(1-e^{-2.303b\left(\varepsilon_{ATZ}[ATZ]+\varepsilon_{O_3}[O_3]+\varepsilon_{H_2O_2}[H_2O_2]+\varepsilon_{HO_2^-}[HO_2^-]\right)}\right)-k_2[O_3]\left[HO_2^-\right]+ \quad (11)$$
$$k_3[O_3][OH^-]-k_7\left[HO_2^-\right][OH\cdot]-k_{24}[NHOH\cdot]\left[HO_2^-\right]$$

$$d[COD]/dt = -k_{19}[COD][OH\cdot]-k_{20}[COD][O_3] \quad (12)$$

$$d[NH_3]/dt = -k_{21}[O_3][NH_3]-k_{22}[NH_3][OH\cdot]-k_{25}[NH_3] \quad (13)$$

where f_{ATZ}, f_{O_3}, $f_{H_2O_2}$, and $f_{HO_2^-}$ are the fractions of UV irradiation absorbed by ATZ, O_3, H_2O_2, and HO_2^-, respectively; b is the optical path length (cm); I and I_0 are the attenuated average irradiance and incident irradiance, respectively (E L^{-1} s^{-1}); α is light attenuation coefficient; k_b and c_b are the extinction coefficient accounting for suspended solids (cm^{-1}) and the number of suspended solids, respectively; k_w is the extinction coefficient accounting for water (cm^{-1}); ε_{ATZ}, ε_{O_3}, $\varepsilon_{H_2O_2}$, and $\varepsilon_{HO_2^-}$ are the molar extinction coefficients of ATZ, O_3, H_2O_2, and HO_2^- at 254 nm, respectively (M^{-1} cm^{-1}); Φ_{ATZ}, Φ_{O_3}, $\Phi_{H_2O_2}$, and $\Phi_{HO_2^-}$ are the quantum yields of ATZ, O_3, and H_2O_2, respectively (mol E^{-1}).

Model parameters and initial conditions are listed in Table 3 by considering (1) incident irradiance was assumed to be homogeneous in the reactor; (2) given that k_w was set as 0.002 cm^{-1} (Luo and Al-Dahhan 2004), the term $k_b c_b$ can be estimated at 0.02 cm^{-1} according to Benson and Rusch (2006); (3) chlorides were assumed to all be NaCl (197,500 mg/L = 5.56 M); (4) the rate constants of COD with O_3 and OH· were set as 0.32 M^{-1} s^{-1} (Rivas et al. 2009; Kwon et al. 2012) and 4.9×10^9 M^{-1} s^{-1} (Mohajerani et al. 2012; Sekaran et al. 2014) based on literature recommendations and trial-and-error testing, respectively; (5) the initial concentration of COD in M was converted from 14,300 mg L^{-1} in Table 1.

The degradation of ATZ, COD, and NH_3 and the individual contributions of various reactive species under different experimental conditions were simulated in MATLAB using function ode15s. The modeling results were then compared with those obtained from experiments to test the accuracy of the proposed kinetic model.

Results and discussion

UV/O_3 treatment efficiency

The removal of COD and NH_3-N by UV/O_3 was found to be best described by pseudo-first-order regression as depicted in Fig. 1. The pseudo-first-order rate constants shown in Eq. 14 were calculated using standard least squares procedures, and all regression coefficients (R^2) were greater than 0.90, indicating reasonable goodness of fit (Table 4).

Table 3 Parameters and initial conditions used for kinetic modeling

	Symbol	Value	Reference
Parameter	ε_{Atz}	3586 M^{-1} cm^{-1}	Luo et al. (2015a)
	$\varepsilon_{H_2O_2}$	19.6 M^{-1} cm^{-1}	Luo et al. (2015a)
	$\varepsilon_{HO_2^-}$	240 M^{-1} cm^{-1}	Andreozzi et al. (1999)
	ε_{O_3}	3600 M^{-1} cm^{-1}	Luo et al. (2015a)
	b	10 cm	Measured
	I_0	2 and 4×10^{-5} E L^{-1} s^{-1}	Estimated*
	kw	0.002 cm^{-1}	Luo and Al-Dahhan (2004)
	$k_b c_b$	0.02 cm^{-1}	Benson and Rusch (2006)
	pH	12	Measured
Initial Conditions	$[ATZ]_0$	2.32×10^{-5} M	Measured
	$[COD]_0$	0.447 M	Measured
	$[NH_3\text{-}N]_0$	1.44×10^{-3} M	Measured
	$[Cl^-]_0$	5.56 M	Measured

*for 7 and 14 W UV irradiation, respectively

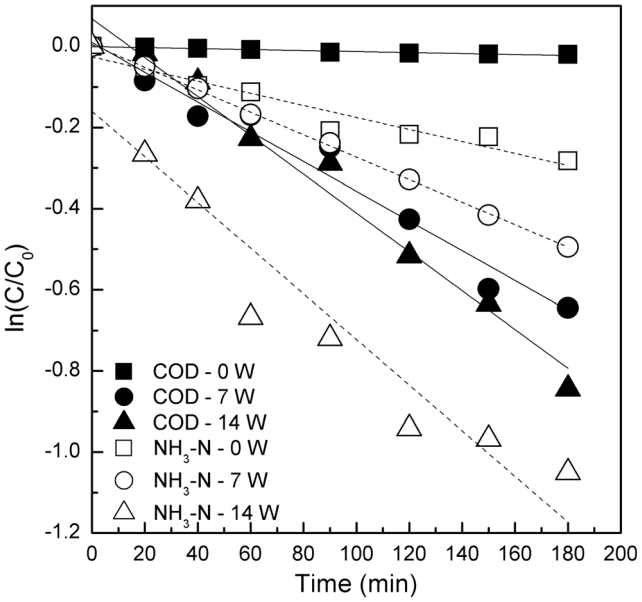

Fig. 1 Pseudo-first-order regression of the removal of COD and NH_3-N using 0, 7, and 14 W UV light (O_3 flow rate at 15 g h^{-1})

$$ln\left(\frac{C_t}{C_0}\right) = -kt \quad (14)$$

where c_t and c_0 are the instant and initial concentrations of COD or NH_3-N (M), respectively; t is time (min); and k is the pseudo-first-order rate constant (min^{-1}). When UV power was set at 0 W, the treatment process was equivalent to sole ozonation and the results showed that 24.6% NH_3-N was removed after 180 min (Fig. 2a), which was consistent with the literature. Zheng et al. (2015b) applied microbubble-ozonation to acrylic fiber manufacturing industry wastewater and found 21% NH_3-N removal efficiencies after 120 min at pH = 8 and an O_3 dose of 5 g h^{-1}. Although O_3 itself can oxidize free NH_3 to nitrate in a relatively slow process (Lester et al. 2013), the abundant hydroxyl ions (OH^-) in the ATZ production wastewater (i.e., pH = 12 in this study) can initiate the decomposition of aqueous O_3 into OH·, which can subsequently degrade NH_3-N (Ozturk and Bal 2015). Similar trend has been reported by Luo et al. (2015b) in treating ammonia-containing wastewater. There was no removal of NH_3-N at a pH of 8 after 120 min ozonation, while an 85% removal was observed at a pH of 12.

Contrastingly, the removal of COD was only about 2% at a rate of 0.0001 min^{-1}. Malik et al. (2017) found a COD removal efficiency of 10–38% to treat complex textile wastewater using 0.1–0.5 g h^{-1} O_3. Wu et al. (2017) also reported that the ozonation of petrochemical secondary effluent can only reduce 13% of the COD with an O_3 dose if 7.9 g h^{-1} within 1 h. Nonetheless, in this study, a 2% reduction of COD at 15 g h^{-1} O_3 dose was considered to be significantly low. This may be attributed to the fact that most organics in the complex wastewater matrix were oxidized selectively by O_3. Some refractory organic matters (e.g., acetic acid and toluene) cannot be detected by the potassium dichromate method but may be degraded to detectable COD by UV photolysis and larger amount of OH· when UV was applied. It also suggests that the generation of OH· via OH^- induced O_3 decomposition (i.e., HO_2^- as an intermediate) may not be sufficient for an effective mineralization of the organics in ATZ production wastewater.

Table 4 Pseudo-first-order rate constants of the removal of COD and NH_3-N (ozone dose at 15 g h^{-1})

UV power (W)	k_{COD} (min^{-1})	R^2	$k_{NH3\text{-}N}$ (min^{-1})	R^2
0	0.0001	0.94	0.0015	0.93
7	0.0037	0.96	0.0028	0.99
14	0.0048	0.97	0.0056	0.90

In real wastewater containing high alkalinity and organic content, the differences between the performance of AOPs are usually more marked (Carra et al. 2016). Therefore, when UV was applied, it can be seen that the removal of both COD and NH_3-N was appreciably enhanced with increasing UV power. The direct photolytic degradation of COD and NH_3-N by UV is generally considered insignificant (Lucas et al. 2010). Therefore, such enhancement is believed to be ascribed to a synergistic effect that the self-decomposition of O_3 is accelerated by UV irradiation, resulting in the generation of more OH·. Hong et al. (2016) also reported COD removal efficiencies of 12.4, 38.9, and 61.6% for the treatment of bio-treated textile wastewater by UV, O_3, and UV/O_3. As OH· formed from O_3 decomposition can considerably oxidize NH_3-N to NO_2^- and further to NO_3^- in alkaline conditions (Huang et al. 2008; Schroeder et al., 2011), the elevation of UV power from 0 to 14 W was able to raise the rate constant of NH_3-N from 0.0015 to 0.0056 min^{-1}. Moreover, applying UV with O_3 was able to substantially enhance the BOD_5/COD ratio. For example, when 14 UV was used, the BOD_5/COD ratio was observed to increase from 0.15 to 0.37 after 180 min treatment, indicating an increase of the biodegradability.

As for ATZ, its removal efficiency was determined to be over 95% after 180 min treatment, regardless the level of UV power. ATZ undergoes fast degradation and is transformed into totally de-alkylated intermediates by ozonation alone, where both direct O_3 attack to the nitrogen or α-carbon atom of the side chains and OH· attack to the α-carbon are involved. ATZ can also be degraded by UV alone through de-chlorination first, where the cleavage of the C–Cl bond occurs at its excited state and then a relatively slow de-alkylation, leading to a greater detoxification rate (Bianchi et al. 2006). Silva et al. (2014) also reported 65–80% removal efficiency with significantly reduced toxicity after 30 min 36 W UV exposure. When applied together, the synergistic effect between UV and O_3 can result in a relatively faster de-alkylation and

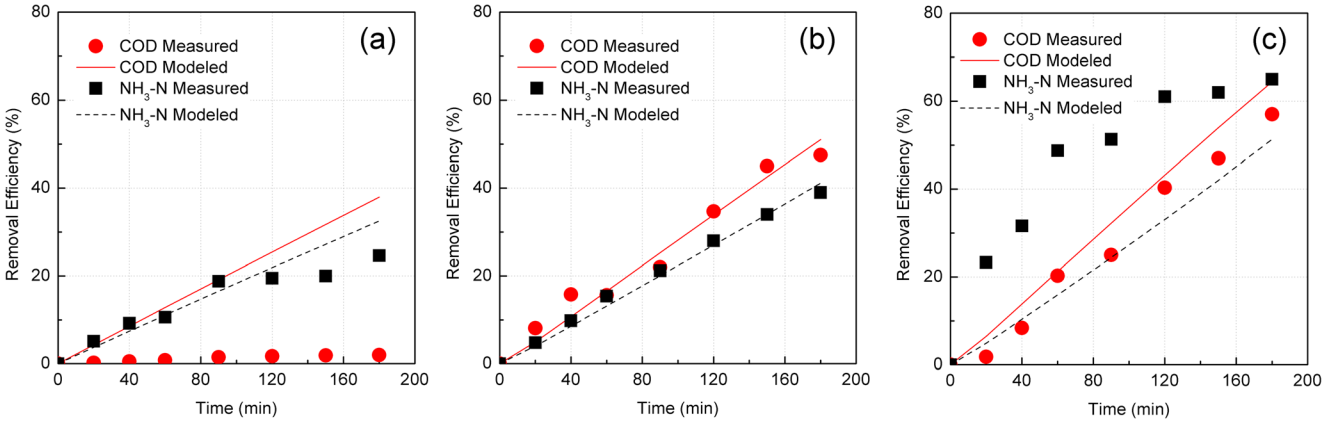

Fig. 2 Comparison between measured and modeled removal of COD and NH_3-N using **a** 0 W, **b** 7 W, and **c** 14 W UV light (O_3 flow rate at 15 g h^{-1})

slower de-chlorination, resulting in the final product of cyanuric acid.

Kinetic modeling of the UV/O_3 system

Figure 2 plots the measured and modeled removal efficiencies of COD and NH_3-N at each sampling point when 0, 7, and 14 W UV was employed. It can be seen that the modeled results agreed well with the measured ones, with root mean square errors (RMSE) of 12.2 and 13.1% for COD and NH_3-N, respectively. The largest discrepancy can be observed in predicting the removal of COD in Fig. 2a and that of NH_3-N in Fig. 2c. In Fig. 2a, the modeled removal efficiencies of COD were higher than the observed ones with a RMSE of 20.3%. One possible reason could be ascribed to the existence of some refractory organic matters, which cannot be detected by the potassium dichromate method but may be degraded to detectable COD when UV was applied (Fig. 2b, c). Another possible explanation is that the amount of OH· formed by OH^- induced O_3 decomposition was not enough, in the experimental system, to achieve a significant mineralization of organics. In addition, pH was not measured during the experiments and was assumed to be unchanged for the ease of model development. Hydroxyl ion-catalyzed O_3 decomposition is highly dependent on the pH of the aqueous system. Treating wastewater by O_3 may slightly reduce pH due to the formation of small molecule organic acids and carbonic acids from the mineralization, which may affect the OH· degradation pathway (Lucas et al. 2010). However, these possible mechanisms were not supported by kinetic modeling as the reduction of COD was modeled as a whole with fixed second-order rate constants, thus causing the discrepancy in Fig. 2a. In Fig. 2c, when 14 W UV was applied, the modeled removal process of NH_3-N was much slower than the measured one. This may be caused by the synergistic effect between UV dose and ozone such that the actual rate constants for NH_3-N removal were higher than the ones listed in Table 2.

The modeled removal efficiencies of ATZ at 0, 7, and 14 W UV after 180 min treatment period were all greater than 95%, which were in good agreement with experimental results. As shown in Fig. 3, when UV was applied, even at a limited power of 7 W, the modeled removal process of ATZ was appreciably accelerated as compared to that of O_3 alone. Such an elevated rate of ATZ degradation can be attributed to two possible mechanisms. One is the extra OH· generated from O_3 decomposition by UV irradiation. According to the insert of Fig. 3, the modeled concentration of OH· increases sharply with the level of UV power applied and is in a range that agrees reasonably with previous research (Zhao et al. 2014; Meng et al. 2017). The other is that higher UV irradiation can increase the possibility of photons being absorbed by ATZ rather than being absorbed, reflected, and scattered by suspended solids. The modeled overall contribution of Cl_2^- ·, OH·, and direct O_3 oxidation to the removal of ATZ was not as comparable as that of direct UV photolysis. Figure 3 plots this contribution by only considering Cl_2^- ·, OH·, and direct O_3

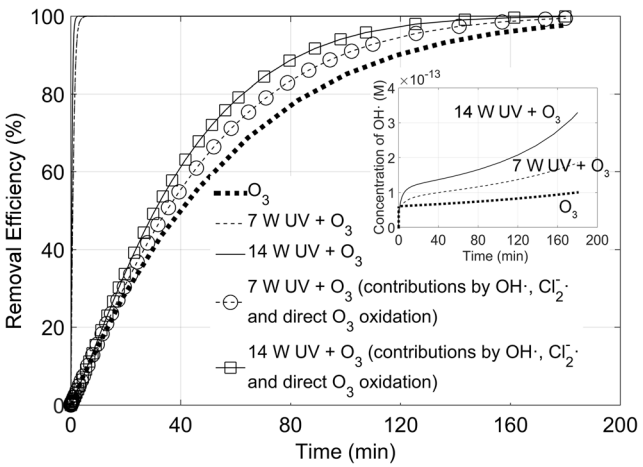

Fig. 3 Modeled removal of ATZ under different experimental conditions (O_3 flow rate at 15 g h^{-1}); calculation of Cl_2^- ·, OH·, and direct O_3 contributions was done by removing the first item UV direct photolysis in Eq. 6)

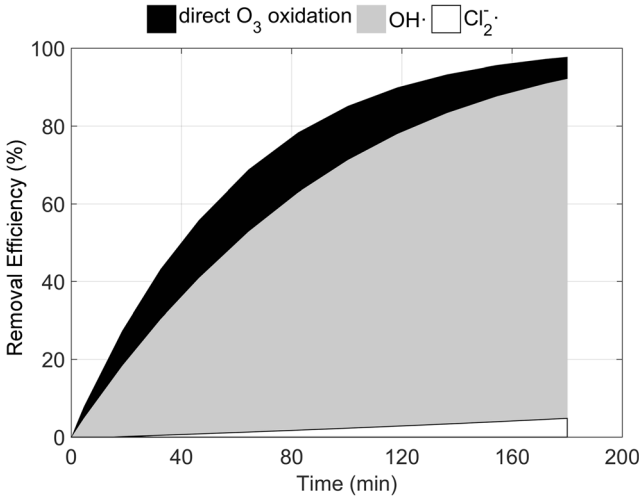

Fig. 4 Contributions of Cl_2^- ·, OH·, and direct O_3 oxidation to the removal of ATZ (UV 0 W, O_3 flow rate at 15 g h^{-1})

oxidation in Eq. 6. For example, the removal efficiency of ATZ at 20 min with 7 W UV was predicted at 99%, whereas this number decreased to 31% by only considering Cl_2^- ·, OH·, and direct O_3 oxidation. The contribution of Cl_2^- ·, OH·, and direct O_3 oxidation to the pseudo-first-order rate constants for the removal of ATZ was around 10% when UV was applied.

Contrastingly, the contributions of Cl_2^- ·, OH·, and direct O_3 oxidation to the removal of ATZ without UV irradiation are plotted in Fig. 4. It can be seen that as long as OH· was taken into account, not considering the contribution from either Cl_2^- · or direct O_3 oxidation did not much affect the removal. This observation implies that in the alkaline environment, the decomposition of O_3 into OH· dominates the direct O_3 oxidation pathway. In addition, the concentration of Cl^- decreased by 0.05% due to scavenging of O_3 and OH·, whereas the contribution of Cl_2^- · to the degradation of ATZ was determined to be negligible, which is consistent with previous reports (Kong et al. 2016).

Contributions of O_3 and OH· to the removal of COD and NH_3-N

To better understand the degradation mechanisms of both COD and NH_3-N in real wastewater systems, the contributions of O_3 and OH· were quantified by the developed kinetic model. The interactions between O_3 and OH· were assumed to be negligible. Figure 5a shows that the removal of COD and NH_3-N caused by direct O_3 oxidation alone appears to be steady at a final proportion of 6.4 and 13.3%, respectively. As a comparison, OH· degrades up to 32.4 and 25.1% of the original amount of COD and NH_3-N in 180 min, respectively. Direct O_3 oxidation is a selective reaction with typical reaction rate constants of 1–1000 M^{-1} s^{-1} (Deng and Zhao, 2015) and usually predominates at pH less than 9. In this study, due to the high pH at 12, OH·-based radical reactions originated from O_3 decomposition would thus dominate.

As depicted by Fig. 5b and c, the higher the UV power, the faster is the decomposition of O_3 and the formation of OH· radicals and thereby the greater the contribution of OH·. The contributions of OH· to the removal of COD and NH_3-N were determined to be 46.7 and 35.5% with 7 W UV and then further increased to 61.4 and 47.5% with 14 W UV. Given the stable contribution of direct O_3 oxidation under different experimental conditions, this finding is in accordance with many previous studies (Laera et al. 2011; Moussavi and Mahdavianpour 2016; Cheng et al. 2016) demonstrating that OH· plays a dominant role for the removal of both COD and NH_3-N in the UV/O_3 system, especially in alkaline environments. By comparing Fig. 5a with Fig. 5b and c, it can be concluded that the contributions of O_3 and OH· at ozonation alone are not as distinguishable as those observed with UV irradiation. This indicates that many other solutes (e.g., Cl^-) may consume OH· in competition with COD and NH_3-N, and such deficiency can be overcome by applying UV irradiation.

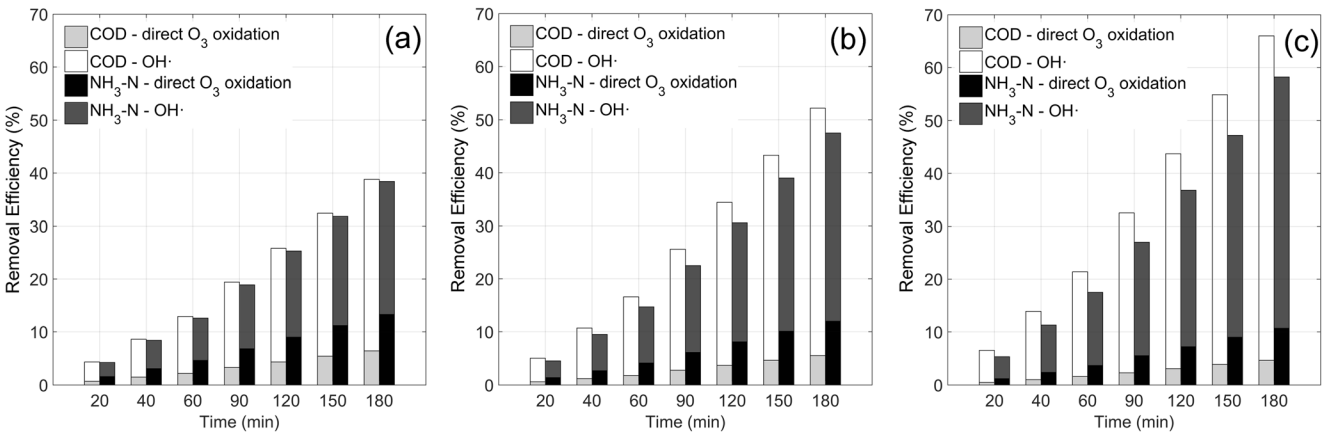

Fig. 5 Modeled contributions of O_3 and OH· on the removal of COD and NH_3-N using **a** 0 W, **b** 7 W, and **c** 14 W UV light (O_3 flow rate at 15 g h^{-1})

Conclusions

The removal of COD, NH_3-N, and ATZ from ATZ production wastewater via UV/O_3 was examined by bench-scale experiments and modeled by reaction kinetics. The following conclusions were drawn and could be valuable for potential scale-up process optimization:

1) The removal of COD and NH_3-N by UV/O_3 followed pseudo-first-order kinetics. For O_3 alone, the low COD removal may be attributed to the existence of certain refractory organic matters, which cannot be detected by the potassium dichromate method but can be degraded by OH· and converted to detectable COD afterwards. When UV was applied, the removal of both COD and NH_3-N was appreciably enhanced.
2) Modeling results agreed reasonably with the experimental data. For COD, the discrepancy maybe due to the presence of refractory organic matters and possible fact that the amount of OH· formed by OH^- induced O_3 decomposition was not enough. As for NH_3-N, the modeling error may be due to the underestimation of its reaction rate constants.
3) According to the modeling results, UV direct photolysis contributed appreciably to the degradation of ATZ, while OH· played a dominant role for the removal of both COD and NH_3-N, especially in alkaline environments.
4) Some possible improvements that could be made for better prediction include continuous O_3 concentration and pH measurement, in situ light attenuation determination, and a detailed analysis of organic composition of the wastewater samples.

Acknowledgements Special thanks go to Natural Sciences and Engineering Research Council of Canada (NSERC), Research and Development Corporation of Newfoundland and Labrador (RDC NL), and Canada Foundation for Innovation (CFI) for supporting this research. Special thanks go to the industrial partners who provided wastewater samples for the experiment.

References

Acero JL, Stemmler K, Von Gunten U (2000) Degradation kinetics of atrazine and its degradation products with ozone and OH radicals: a predictive tool for drinking water treatment. Environ Sci Technol 34(4):591–597. https://doi.org/10.1021/es990724e

Andreozzi R, Caprio V, Insola A, Marotta R (1999) Advanced oxidation processes (AOP) for water purification and recovery. Catal Today 53(1):51–59. https://doi.org/10.1016/S0920-5861(99)00102-9

Aquino JM, Miwa DW, Rodrigo MA, Motheo AJ (2017) Treatment of actual effluents produced in the manufacturing of atrazine by a photo-electrolytic process. Chemosphere 172:185–192. https://doi.org/10.1016/j.chemosphere.2016.12.154

Beltrán FJ, García-Araya JF, Acedo B (1994) Advanced oxidation of atrazine in water—II. Ozonation combined with ultraviolet radiation. Water Res 28(10):2165–2174. https://doi.org/10.1016/0043-1354(94)90028-0

Beltrán FJ, González M, Acedo B, Rivas FJ (2000) Kinetic modelling of aqueous atrazine ozonation processes in a continuous flow bubble contactor. J Hazard Mater 80(1):189–206. https://doi.org/10.1016/S0304-3894(00)00302-2

Beltrán FJ, González M, Rivas FJ, Alvarez P (1996) Aqueous UV radiation and UV/H_2O_2 oxidation of atrazine first degradation products: deethylatrazine and deisopropylatrazine. Environ Toxicol Chem 15(6):868–872. https://doi.org/10.1002/etc.5620150607

Benson BC, Rusch KA (2006) Investigation of the light dynamics and their impact on algal growth rate in a hydraulically integrated serial turbidostat algal reactor (HISTAR). Aquac Eng 35(2):122–134. https://doi.org/10.1016/j.aquaeng.2005.09.005

Bianchi CL, Pirola C, Ragaini V, Selli E (2006) Mechanism and efficiency of atrazine degradation under combined oxidation processes. Appl Catal B 64(1):131–138. https://doi.org/10.1016/j.apcatb.2005.11.009

Bielski BH (1993) A pulse radiolysis study of the reaction of ozone with Cl_2^- in aqueous solutions. Radiat Phys Chem 41(3):527–530

Bu L, Shi Z, Zhou S (2016) Modeling of Fe(II)-activated persulfate oxidation using atrazine as a target contaminant. Sep Purif Technol 169:59–65

Buxton GV, Greenstock CL, Helman WP, Ross AB (1988) Critical review of rate constants for reactions of hydrated electrons, hydrogen atoms and hydroxyl radicals (·OH/·O^-) in aqueous solution. J Phys Chem Ref Data 17(2):513–886

Carra I, Sánchez Pérez JA, Malato S, Autin O, Jefferson B, Jarvis P (2016) Performance of different advanced oxidation processes for tertiary wastewater treatment to remove the pesticide acetamiprid. J Chem Technol Biot 91(1):72–81

Cheng J, Ye Q, Xu J, Yang Z, Zhou J, Cen K (2016) Improving pollutants removal by microalgae Chlorella PY-ZU1 with 15% CO_2 from undiluted anaerobic digestion effluent of food wastes with ozonation pretreatment. Bioresour Technol 216:273–279

da Costa Filho BM, da Silva VM, de Oliveira SJ, da Hora Machado AE, Trovó AG (2016) Coupling coagulation, flocculation and decantation with photo-Fenton process for treatment of industrial wastewater containing fipronil: biodegradability and toxicity assessment. J Environ Manage 174:71–78

Deng Y, Zhao R (2015) Advanced oxidation processes (AOPs) in wastewater treatment. Current Pollution Reports 1(3):167–176

Fang J, Fu Y, Shang C (2014) The roles of reactive species in micropollutant degradation in the UV/free chlorine system. Environ Sci Technol 48(3):1859–1868

Garoma T, Gurol MD (2004) Degradation of tert-butyl alcohol in dilute aqueous solution by an O_3/UV process. Environ Sci Technol 38(19):5246–5252

Gassie LW, Englehardt JD, Wang J, Brinkman N, Garland J, Gardinali P, Guo T (2016) Mineralizing urban net-zero water treatment: phase II field results and design recommendations. Water Res 105:496–506

Gomes J, Costa R, Quinta-Ferreira RM, Martins RC (2017) Application of ozonation for pharmaceuticals and personal care products removal from water. Sci Total Environ 586:265–283

Haag WR, Hoigne J, Bader H (1984) Improved ammonia oxidation by ozone in the presence of bromide ion during water treatment. Water Res 18:1125–1128

Hong T, Dang Y, Zhou D, Hu Y (2016) Study on the oxidative characteristics of organics in bio-treated textile wastewater by VUV/US/O_3 process. Chem Eng J 306:560–567

Horikoshi S, Hidaka H (2003) Non-degradable triazine substrates of atrazine and cyanuric acid hydrothermally and in supercritical water under the UV-illuminated photocatalytic cooperation. Chemosphere 51(2):139–142

Huang L, Li L, Dong W, Liu Y, Hou H (2008) Removal of ammonia by OH radical in aqueous phase. Environ Sci Technol 42(21):8070–8075

Jing L, Chen B, Zhang BY, Li P (2015) Process simulation and dynamic control for marine oily wastewater treatment using UV irradiation. Water Res 81:101–112

Jing L, Chen B, Wen DY, Zheng JS, Zhang BY (2017) Pilot-scale treatment of atrazine production wastewater by UV/O 3 /ultrasound: Factor effects and system optimization. J Environ Manage 203: 182–190

Kang N, Jackson WA, Dasgupta PK, Anderson TA (2008) Perchlorate production by ozone oxidation of chloride in aqueous and dry systems. Sci Total Environ 405(1):301–309

Khan JA, He X, Shah NS, Khan HM, Hapeshi E, Fatta-Kassinos D, Dionysiou DD (2014) Kinetic and mechanism investigation on the photochemical degradation of atrazine with activated H_2O_2, $S_2O_8^{2-}$ and HSO_5^-. Chem Eng J 252:393–403

Khuntia S, Majumder SK, Ghosh P (2012) Removal of ammonia from water by ozone microbubbles. Ind Eng Chem Res 52(1):318–326

Kong X, Jiang J, Ma J, Yang Y, Liu W, Liu Y (2016) Degradation of atrazine by UV/chlorine: efficiency, influencing factors, and products. Water Res 90:15–23

Kwon SC, Kim JY, Yoon SM, Bae W, Kang KS, Rhee YW (2012) Treatment characteristic of 1, 4-dioxane by ozone-based advanced oxidation processes. Ind Eng Chem Res 18(6):1951–1955

Laera G, Cassano D, Lopez A, Pinto A, Pollice A, Ricco G, Mascolo G (2011) Removal of organics and degradation products from industrial wastewater by a membrane bioreactor integrated with ozone or UV/H_2O_2 treatment. Environ Sci Technol 46(2):1010–1018

Lester Y, Mamane H, Zucker I, Avisar D (2013) Treating wastewater from a pharmaceutical formulation facility by biological process and ozone. Water Res 47:4349–4356

Lucas MS, Peres JA, Puma GL (2010) Treatment of winery wastewater by ozone-based advanced oxidation processes (O_3, O_3/UV and O_3/UV/H_2O_2) in a pilot-scale bubble column reactor and process economics. Sep Purif Technol 72(3):235–241

Luo HP, Al-Dahhan MH (2004) Analyzing and modeling of photobioreactors by combining first principles of physiology and hydrodynamics. Biotechnol Bioeng 85(4):382–393

Luo C, Ma J, Jiang J, Liu Y, Song Y, Yang Y, Guan Y, Wu D (2015a) Simulation and comparative study on the oxidation kinetics of atrazine by UV/H_2O_2, UV/HSO_5^- and UV/$S_2O_8^{2-}$. Water Res 80:99–108

Luo X, Yan Q, Wang C, Luo C, Zhou N, Jian C (2015b) Treatment of ammonia nitrogen wastewater in low concentration by two-stage ozonization. Int J Environ Res Public Health 12(9):11,975–11, 987

Lutze HV, Bircher S, Rapp I, Kerlin N, Bakkour R, Geisler M, Schmidt TC (2015) Degradation of chlorotriazine pesticides by sulfate radicals and influence of organic matter. Environ Sci Technol 49(3): 1673–1680

Malik SN, Ghosh PC, Vaidya AN, Waindeskar V, Das S, Mudliar SN (2017) Comparison of coagulation, ozone and ferrate treatment processes for color, COD and toxicity removal from complex textile wastewater. Wat Sci Tech wst2017062

Manenti DR, Soares PA, Módenes AN, Espinoza-Quiñones FR, Boaventura RA, Bergamasco R, Vilar VJ (2015) Insights into solar photo-Fenton process using iron (III)–organic ligand complexes applied to real textile wastewater treatment. Chem Eng J 266:203–212

Matthew BM, Anastasio C (2006) A chemical probe technique for the determination of reactive halogen species in aqueous solution: Part 1–bromide solutions. Atmos Chem Phys 6(9):2423–2437

Meng L, Yang S, Sun C, He H, Xian Q, Li S, Wang G, Zhang L, Jiang D (2017) A novel method for photo-oxidative degradation of diatrizoate in water via electromagnetic induction electrodeless lamp. J Hazard Mater 337:34–46

Mohajerani M, Mehrvar M, Ein-Mozaffari F (2012) Photoreactor design and CFD modelling of a UV/H_2O_2 process for distillery wastewater treatment. Can J Chem Eng 90:719–729

Moussavi G, Mahdavianpour M (2016) The selective direct oxidation of ammonium in the contaminated water to nitrogen gas using the chemical-less VUV photochemical continuous-flow reactor. Chem Eng J 295:57–63

Neta P, Huie RE, Ross AB (1988) Rate constants for reactions of inorganic radicals in aqueous solution. J Phys Chem Ref Data 17(3): 1027–1284

Ozturk E, Bal N (2015) Evaluation of ammonia–nitrogen removal efficiency from aqueous solutions by ultrasonic irradiation in short sonication periods. Ultrason Sonochem 26:422–427

Park S, Kim M (2015) Innovative ammonia stripping with an electrolyzed water system as pretreatment of thermally hydrolyzed wasted sludge for anaerobic digestion. Water Res 68:580–588

Pophali GR, Hedau S, Gedam N, Rao NN, Nandy T (2011) Treatment of refractory organics from membrane rejects using ozonation. J Hazard Mater 189(1):273–277

Prieto-Rodríguez L, Oller I, Klamerth N, Agüera A, Rodríguez EM, Malato S (2013) Application of solar AOPs and ozonation for elimination of micropollutants in municipal wastewater treatment plant effluents. Water Res 47(4):1521–1528

Quero-Pastor MJ, Garrido-Perez MC, Acevedo A, Quiroga JM (2014) Ozonation of ibuprofen: a degradation and toxicity study. Sci Total Environ 466:957–964

Rivas J, Gimeno O, Beltrán F (2009) Wastewater recycling: application of ozone based treatments to secondary effluents. Chemosphere 74(6): 854–859

Schroeder JP, Croot PL, Von Dewitz B, Waller U, Hanel R (2011) Potential and limitations of ozone for the removal of ammonia, nitrite, and yellow substances in marine recirculating aquaculture systems. Aquacult Eng 45(1):35–41

Sekaran G, Karthikeyan S, Boopathy R, Maharaja P, Gupta VK, Anandan C (2014) Response surface modeling for optimization heterocatalytic Fenton oxidation of persistence organic pollution in high total dissolved solid containing wastewater. Environ Sci Pollut R 21(2):1489–1502

Silva MP, dos Santos Batista AP, Borrely SI, Silva VHO, Teixeira ACSC (2014) Photolysis of atrazine in aqueous solution: role of process variables and reactive oxygen species. Environ Sci Pollut R 21(21): 12,135–12,142

Staehelin J, Hoigne J (1982) Decomposition of ozone in water: rate of initiation by hydroxide ions and hydrogen peroxide. Environ Sci Technol 16(10):676–681

Wen Q, Zhang S, Chen Z, Wang J (2016) Using powdered activated carbon to enhance atrazine removal in an anoxic/oxic (A/O) process. Desalin Water Treat 57(27):12,700–12,707

Wu C, Zhou Y, Wang Y, Guo M (2017) Innovative combination of Fe^{2+}-BAF and ozonation for enhancing phosphorus and organic micropollutants removal treating petrochemical secondary effluent. J Hazard Mater 323:654–662

Xu LJ, Chu W, Graham N (2014) Atrazine degradation using chemical-free process of USUV: analysis of the micro-heterogeneous environments and the degradation mechanisms. J Hazard Mater 275:166–174

Yang Y, Cao H, Peng P, Bo H (2014) Degradation and transformation of atrazine under catalyzed ozonation process with TiO_2 as catalyst. J Hazard Mater 279:444–451

Yu XY, Barker JR (2003) Hydrogen peroxide photolysis in acidic aqueous solutions containing chloride ions. I. Chemical mechanism. J Phys Chem A 107(9):1313–1324

Zhao C, Arroyo-Mora LE, DeCaprio AP, Sharma VK, Dionysiou DD, O'Shea KE (2014) Reductive and oxidative degradation of iopamidol, iodinated X-ray contrast media, by Fe (III)-oxalate under UV and visible light treatment. Water Res 67:144–153

Zheng JS, Liu B, Ping J, Chen B, Wu HJ, Zhang BY (2015a) Vortex- and shaker-assisted liquid–liquid microextraction (VSA-LLME) coupled with gas chromatography and mass spectrometry (GC-MS) for analysis of 16 polycyclic aromatic hydrocarbons (PAHs) in offshore produced water. Water Air Soil Poll 226:318–331

Zheng T, Wang Q, Zhang T, Shi Z, Tian Y, Shi S, Smale N, Wang J (2015b) Microbubble enhanced ozonation process for advanced treatment of wastewater produced in acrylic fiber manufacturing industry. J Hazard Mater 287:412–420

Zhou S, Bu L, Shi Z, Bi C, Yi Q (2016) A novel advanced oxidation process using iron electrodes and ozone in atrazine degradation: performance and mechanism. Chem Eng J 306:719–725